Chemical Physics 396 (2012) 72–83

Contents lists available at SciVerse ScienceDirect

Chemical Physics

journal homepage: www.elsevier.com/locate/chemphys

Time-resolved FTIR spectroscopy for monitoring protein dynamics exemplified by functional studies of Ras protein bound to a lipid bilayer

Carsten Kötting *, Jörn Güldenhaupt, Klaus Gerwert *

Lehrstuhl für Biophysik, Ruhr-Universität Bochum, D-44780 Bochum, Germany

ARTICLE INFO

Article history:
Available online 22 August 2011

Keywords:
Infrared
Time-resolved
Difference spectroscopy
Rapid scan
Step scan
GTPases
GTP
Caged-substances
Ras
Isotopic labeling
Band assignment
Global fit
Attenuated total reflection (ATR)
Monolayer
Solid supported lipid bilayer (SSLB)

ABSTRACT

Time-resolved Fourier transform infrared (FTIR) difference spectroscopy is a valuable tool for monitoring the dynamics of protein reactions and interactions. Absorbance changes can be monitored with time resolutions down to nanoseconds and followed for time periods that range over nine orders of magnitude. Membrane proteins bound to solid supported lipid bilayers can be investigated in near physiological conditions with the attenuated total reflection (ATR) technique. Here, we review the basics of time-resolved FTIR with a focus on Ras, a GTPase that is mutated in 25% of human tumors. We show the first time-resolved measurements of membrane anchored Ras and observed the switching between its activated and its inactivated state. We compared those measurements with measurements of the truncated Ras in solution. We found that both the kinetics and the functional groups involved were very similar. This suggested that the membrane did not have a major influence on the hydrolysis reaction.

1. Outline

This paper combines a broad introduction into time resolved FTIR spectroscopy with new results on membrane bound Ras proteins. Time-resolved FTIR spectroscopy is reviewed in several books [1,2] and journals [3,4]. In the following Section 2, we show the basics and the setup of a FTIR spectrometer, including various sample cells, and the concept of difference spectroscopy. We discuss triggering techniques and both the rapid scan and the step scan technology followed by methods for data evaluation and band assignment. This chapter ends with a discussion on ATR–FTIR spectroscopy. In the next Section 3, we introduce the GTPase Ras and highlight results obtained by time resolved FTIR measurements of Ras in solution. Next (Section 4), we describe the first time resolved experiments of a GTPase in its native environment, anchored at a membrane by ATR–FTIR spectroscopy. These new results and the new experimental capabilities of this novel setup are discussed. Experimental details are given in the final Section 5.

2. Introduction into time-resolved FTIR spectroscopy

2.1. General setup of a time-resolved FTIR spectrometer

A typical setup for a time-resolved FTIR experiment is shown in Fig. 1A. The light source is a globar (SiC heated to 1800 K), which is a black body radiator. Its infrared light passes through an aperture (0.25–12 mm) before entering a Michelson interferometer, which consists of a beamsplitter (KBr for mid-infrared), a fixed mirror, and a movable mirror. Subsequently, the light passes through the sample chamber, which can be equipped, e.g., with a thermostatic transmission cell. This cell can additionally be irradiated with a laser. Finally, the infrared light reaches a liquid nitrogen-cooled MCT (mercury, cadmium and telluride, HgCdTe)-detector.

FTIR spectrometers have crucial advantages over dispersive spectrometers. With a Michelson interferometer (Fig. 1B), all wavelengths can be measured in parallel (multiplex advantage). At the beamsplitter, one half of the infrared light is reflected to a fixed mirror, and the other half is transmitted to a movable mirror. Both beams are reflected back and recombined at the beamsplitter. The positions of the fixed and movable mirrors can be at different distances from the beamsplitter; this leads to a path difference (ΔX). For example, a path difference of zero between two

* Corresponding authors.
E-mail addresses: carsten.koetting@rub.de (C. Kötting), gerwert@bph.rub.de (K. Gerwert).

0301-0104/$ - see front matter © 2011 Elsevier B.V. All rights reserved.
doi:10.1016/j.chemphys.2011.08.007

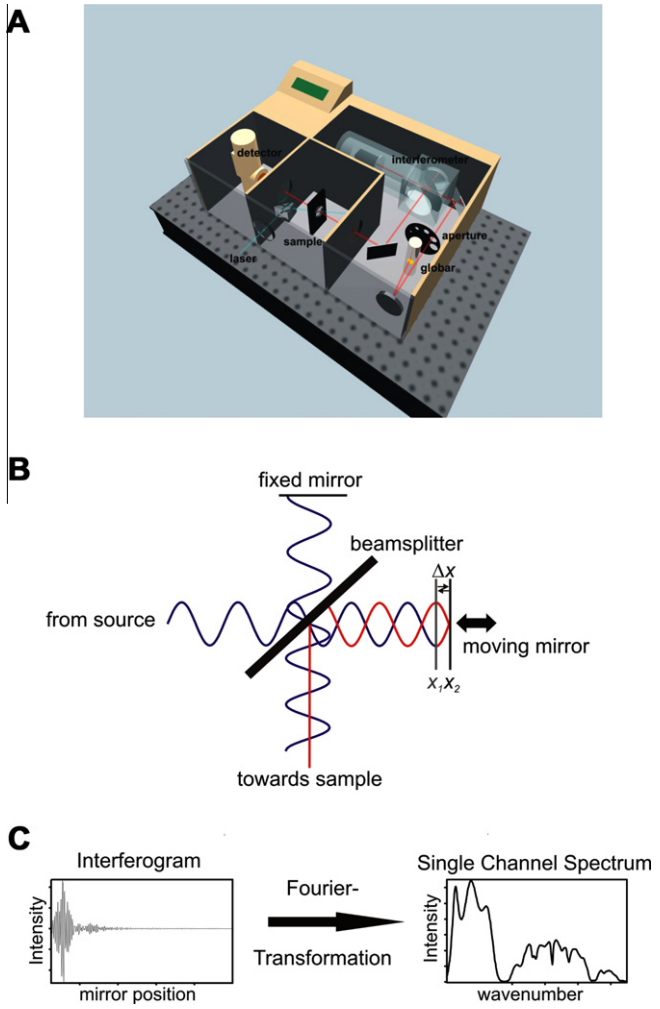

Fig. 1. (A) Schematic of an FTIR spectrometer on a vibration isolation table [73]. (B) Schematic representation of a Michelson interferometer. An electromagnetic wave is split at the beamsplitter; one half is reflected to a fixed mirror, the other half is transmitted to a movable mirror. Both parts are recombined at the beamsplitter. For mirror position X_1, the path difference, ΔX, is zero and the wave interferes constructively; for mirror position X_2, the path difference, ΔX, is half a wavelength, and thus, the inference is destructive. (C) The result of the measurement is an interferogram, where the intensity is plotted against the mirror position. After Fourier transformation, the intensity I is obtained as a function of the wavelength (single channel spectrum) [74].

monochromatic waves (movable mirror at position X_1) leads to constructive interference; a path difference of half a wavelength (movable mirror at position X_2) leads to extinction. By varying the path difference (by moving the movable mirror), the interference pattern of polychromatic light after recombination leads to an interferogram. The interferogram is a plot of the intensity at the detector against the mirror position. After Fourier transformation, the intensity I as a function of the wavelength is obtained (single channel transmittance spectrum, Fig. 1C). An absorbance spectrum A is obtained by comparing two single channel transmittance spectra, one with a sample (I) and one without a sample (I_0), according to the following equation:

$$A = -\log\frac{I}{I_0}.$$

With modern FTIR spectrometers, a complete spectrum can be obtained within 10 ms. Further advantages of FTIR spectrometers are the absence of dispersive elements (slits combined with prisms or gratings that attenuate the signal intensity; the Jaquinot advantage), and the high accuracy of the wavelength (Connes advantage).

Some sample cells are shown in Fig. 2. The most common cell is a simple transmission cell with IR-transparent windows (e.g., CaF_2) as shown in Fig. 2A. Due to the high absorptivity of water in the mid-infrared spectral region, meaningful spectra of hydrated proteins can only be obtained by transmission measurements through very thin (2–10 μm) films. This involves placing a drop of protein in suspension or solution onto an IR transparent window and then carefully concentrating it under a nitrogen stream or under vacuum. Alternatively, a suspension of a membrane–protein can be centrifuged and the pellet can then be squeezed between two IR transparent windows. A typical measurement requires about 100–200 μg protein. The concentration of the protein in the film is 2–10 mM. The sample chamber is closed with a second IR-window, which is separated from the first by a mylar-spacer that is a few μm thick.

Alternatively, ATR cells (Fig. 2B) can be used instead of transmission cells [5,6] (For details see Section 2.7). Both transmission cells and ATR-cells can be used as flowcells (Fig. 2C). Here, the sample can be exchanged with another sample by means of a tubing system. This can increase the quality of the difference spectra enormously, because the whole setup (sample thickness, window position, etc.) can be maintained exactly the same for different samples.

Silicon is transparent in the mid-infrared range. Therefore, micromachined silicon components offer great potential for FTIR spectroscopy, particularly for studying microsecond mixing experiments [7]. In these devices, a protein solution is placed between two streams of mixing buffer to form a laminar flow pattern. Because the protein layer is thin, diffusing reactant molecules (e.g., ligands) stream from the buffer solution into the protein solution within microseconds. The induced reaction can be monitored with high time resolution by scanning along an observation channel downstream of the mixing area with the focused beam of a FTIR microscope.

Fig. 3 shows the absorbance spectrum of a protein. A small protein of 20 kD has about 10^4 absorbance bands in the infrared region. Thus, from the absorption spectrum alone, one cannot obtain information on individual bands; it is only possible to determine global features of the protein. The spectrum is dominated by amide I (C=O stretch) and amide II (NH bend coupled with C–N stretch) bands, which are present in every amino acid. From this backbone absorption, information on the secondary structure can be gained [8,9]. Water absorptions (O–H bend) are found in the same region as amide I.

For a FTIR difference spectrum of reaction A → B, one calculates the absorbance spectrum of B minus the absorbance spectrum of A. Thus, the vibrations from groups that did not change during the reaction will cancel each other out, and the remaining bands represent only the changes in absorbance that occurred during the reaction (Fig. 3, inset). Now, individual residues can be resolved. It is important that the same conditions are accurately maintained during the reactions; otherwise the background, with a $\sim 10^3$ times stronger absorbance, will obscure the difference spectrum. Highly sensitive instrumentation is required to monitor these very small changes. FTIR spectroscopy is able to reliably detect small changes, due to the multiplex and the Jacquinot advantages, which increase the signal to noise ratio.

2.2. Trigger techniques for time-resolved FTIR

The changes in absorbance due to a reaction are several orders smaller than the background absorbance of the protein; therefore, the difference technique requires a sharp initiation (triggering) of the protein reaction, and this activation must be achieved without

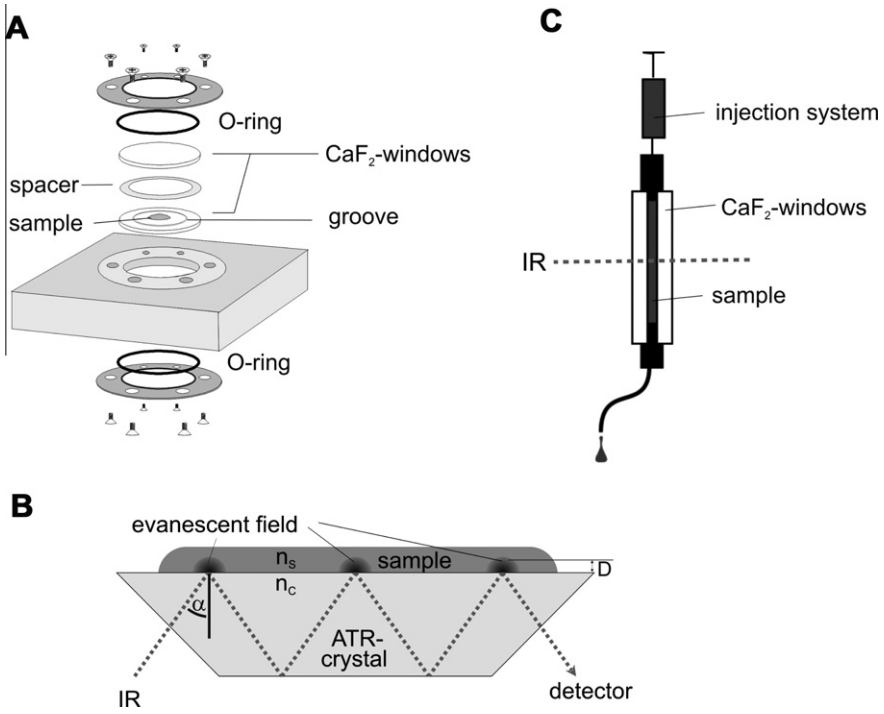

Fig. 2. Various sample cells. (A) Transmission cell. Instead of a spacer, windows with a polished well can be used; (C) ATR cell. Only the region close to the crystal is monitored; (B) flowcell. The sample can be exchanged without taking the cell out of the spectrometer; this provides increased sensitivity [74].

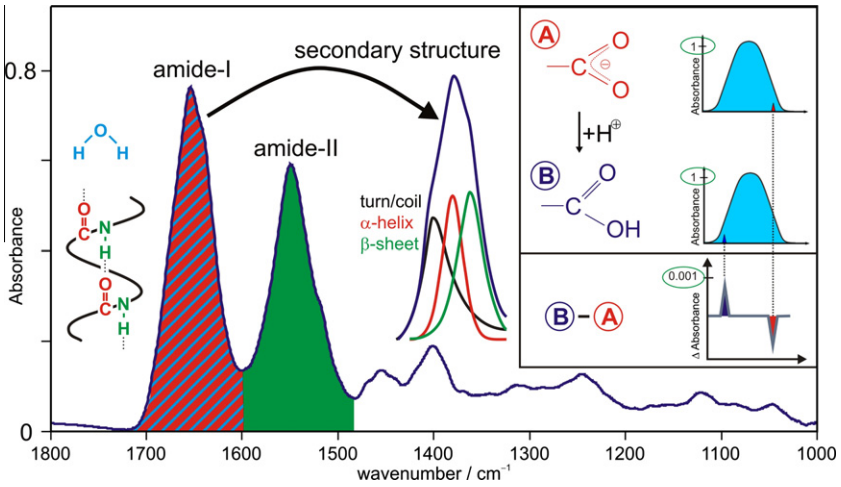

Fig. 3. Typical IR absorbance spectrum of a protein in solution (Ras). The main components are indicated by the colors: red indicates a C=O stretching vibration, amide I; blue indicates the bending vibration of water; and green indicates a combination of NH bending and CN stretching vibrations, amide II. In the inset, two absorption spectra of a protein are shown schematically; the two spectra deviate only in the protonation of a carboxyl group. In the lower part, a difference spectrum of these two states is shown schematically. The background absorptions of the unchanged part of the protein are cancelled out; the absorptions of the reacting group are resolved [74].

removing the sample from the chamber. The activation can be achieved by photoexcitation or by fast mixing.

2.2.1. Photobiological systems

Light-induced reactions in photobiological systems are ideally suited to time-resolved studies. For example, in bacteriorhodopsin (bR) [10,11] and photosynthetic reaction centers (RCs), [12] which carry intrinsic chromophores, the chromophore can be directly activated with a laser flash. This induces isomerisation or redox reactions in the prosthetic groups.

2.2.2. Redox active systems

By applying an electrical potential in a spectroelectrochemical cell redox-linked conformational changes of proteins can be monitored. This combined technique allows for investigating redox active proteins e.g. proteins from the respiratory chain (cytochrome *c*, cytochrome *c* oxidase) or hydrogenases [13–15].

2.2.3. Caged compounds

A much broader range of applications can be achieved with caged compounds. These compounds release biologically active molecules from inactive photolabile precursors. This allows the initiation of a protein reaction; for example, inactive precursors can be activated with a nanosecond UV laser flash. In addition, caged phosphate, caged GTP, caged ATP, and caged calcium have been established as particularly suitable trigger compounds [16–19]. Furthermore, caged glutamic acid [20] and caged protons [21] have been described. The most popular caging groups are

ortho-alkylated nitrophenyl compounds [22]. However, these photoreactions involve several intermediates, which limit the time resolution for the reaction. A higher time resolution is achievable with the *para*-hydroxyphenacyl-cage; that reaction proceeds on the excited state in the subnanosecond time range [23].

2.3. Rapid scan

The rapid scan FTIR mode of time-resolved spectroscopy permits observation of processes that have a half-life on the order of the scan time, or less, for first-order reactions. The principle of the rapid scan technique is simple: after taking a reference spectrum of the protein in its ground state, one activates the protein (e.g., with a laser flash) and records interferograms in much shorter intervals than the half-lives of the reactions [11]. The time pattern of a rapid scan experiment is shown schematically in Fig. 4A–C. The reference (R) interferograms represent the educt state (A). With a laser flash, the protein or ligand becomes activated, e.g., by removing a cage group. Then, the reaction can be monitored by taking interferograms during the complete reaction pathway (B to C to D). Thus, the first interferogram after the flash will mainly represent the spectrum of B; in the following interferograms, the ratio of C will increase according to the kinetics of the observed reaction. A global exponential fit or multivariate curve resolution (MCR) analysis (see below) produces the difference spectra for each reaction step (Fig. 4C). When the half-life of the observed process is shorter than the duration of the scan, the intensity of the interferogram can be convolved with the absorption change of the sample. In the case of first-order reactions, the interferogram is convolved with an exponential function, which results in Lorentzian line shape broadening in the spectrum after Fourier transformation.

2.4. Step scan

Much higher time-resolution can be achieved with the step scan technique. In the step scan mode, the movable mirror in the interferometer is held stationary at position x_n (Fig. 5); the protein activity is initiated, for example, with a laser flash, and the time dependence of the intensity change at this interferogram position x_n is measured. Then, the movable mirror is "stepped" to the next data position, x_{n+1}, and the reaction is repeated and measured again. This process is continued at each sampling position. The position of the interferometer mirror must be accurately maintained to within 1–2 nm of x_n during the reaction time. Therefore, the method is very sensitive to external disturbances (e.g., noise). Furthermore, the experimental conditions must be the same for all mirror positions. This can easily be achieved for a cyclic reaction, like the photocycle of bacteriorhodopsin. For non-cyclic reactions, either the sample must be exchanged for each mirror position [24] or a homogenous sample must be probed in small segments with a focused beam [25].

The time resolution is usually determined by the response time of the detector, which is typically a few nanoseconds. After the measurement, the data is rearranged to yield time-dependent interferograms $I(t_i)$. When pulsed IR sources are used instead of the conventional globar, the time resolution is determined by the time duration of the probe pulse. This can, in principle, provide femtosecond resolution with broad band femtosecond lasers or synchrotron radiation. For more details on the step scan technique, see the following literature [26–30].

2.5. Global fit

For analyzing time-resolved data, adequate kinetic analysis is important. A so-called global-fit analysis yields the apparent rate constants of the analyzed processes [31]. The global-fit analysis not only fits the absorbance change at a specific wavenumber, but simultaneously fits the changes within the complete spectrum. All reactions are assumed to be first order, and therefore, they can be described by a sum of exponentials. The fit procedure minimizes the difference between the measured data $\Delta A_{measured}$ and the theoretical description ΔA, shown in the equation below. ΔA is weighted according to the noise w_{ij} at the respective wavenumbers, and summed over time (t) and over the wavenumbers (ν). Thus, the change in absorbance, ΔA, is the sum of n_r exponentials, with apparent rate constants k_l, and amplitudes a_l:

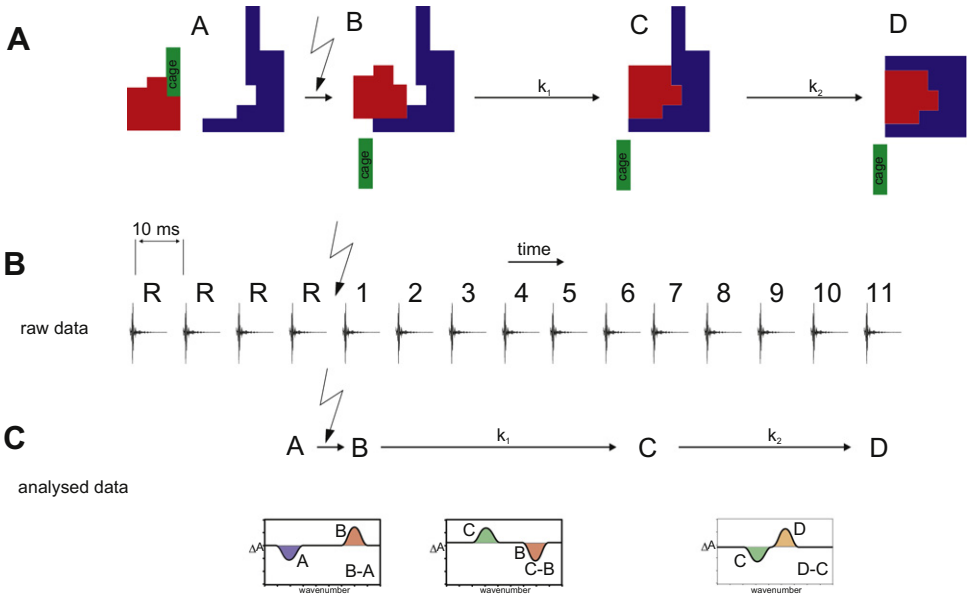

Fig. 4. (A) Time course from a rapid scan FTIR experiment. The laser flash removes the cage group (green), which allows an interaction between the protein (blue) and the ligand (red). This leads to the formation of the protein–ligand complex (D) via the intermediate (C). (B) Time course of data acquisition: first, reference spectra (R) are taken. The laser flash initiates a reaction. During the reaction from B via C to D, interferograms are recorded. (C) Analysis of the time resolved data allows the calculation of difference spectra; these show the bands of groups involved in the subsequent reaction steps [74].

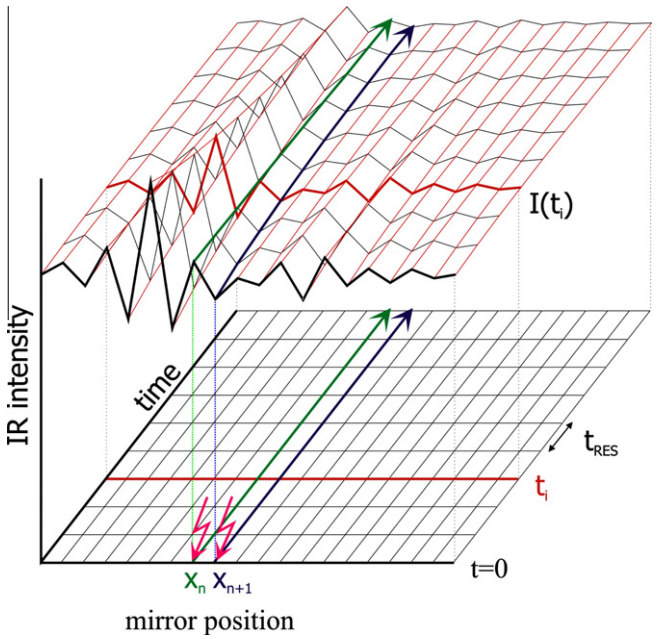

Fig. 5. Principles of the step scan technique. The interferometer mirror is stepped to a sampling position, x_n; the reaction is then initiated, and the time dependence of the IR intensity is measured (green arrow). The detector limits the time resolution. After relaxation, the interferometer is stepped to the next position, x_{n+1}, and the data recording process is repeated (blue arrow). After measurements at all interferometer positions, the data is rearranged to yield time-dependent interferograms $I(t_i)$ (red); these are subjected to Fourier transformation to yield the time-dependent spectra [74].

$$\Delta A(\nu,t) = \sum_{l=1}^{n_r} a_l(\nu)e^{-k_l t} + a_\infty(\nu).$$

This analysis minimizes the weighted sum of squared differences, f (shown below), between the fit, with n_r apparent rate constants (k_l) and the data points at n_w measured wavenumbers (ν_i) and n_t times (t_j).

$$f = \sum_{i=1}^{n_w}\sum_{j=1}^{n_t}(w_{ij})^2(\Delta A_{measured}(\nu_i,t_j) - \sum_{l=1}^{n_r} a_l(\nu_i)e^{-k_l t} + a_\infty(\nu_i))^2.$$

For unidirectional forward reactions, the determined apparent rate constants are directly related to the respective intrinsic rate constants that describe the respective reaction steps [32,33]. In addition, when significant back-reactions occur, the analysis becomes more complicated [34]. Then, the reaction must be modeled with sufficient intrinsic rate constants to fulfill the experimentally observed time-course described by the apparent rate constants. Because the number of intrinsic rate constants in the model is larger than the number of experimentally observed apparent rate constants, the problem is experimentally underdetermined, and the solution is not unequivocal.

An alternative is the multivariate curve resolution (MCR) method [35]. In the MCR method, the difference spectra of the pure intermediates and their concentration profiles are calculated from all the measured difference spectra. This procedure allows the determination of transient spectra, independent of specific kinetic models and independent of the temporal overlap [31].

2.6. Band assignments

In order to derive information on the mechanism of a protein reaction or interaction, the infrared bands have to be assigned to individual groups of the protein or the ligand. The frequency range in which a band appears allows a rough tentative assignment of the bands. For example, asymmetric phosphate stretching vibrations are expected in the region between 1250 cm^{-1} and 1050 cm^{-1}, and the carbonyl vibrations of the protein backbone are found between 1700 cm^{-1} and 1600 cm^{-1} (amide I). Band assignment can be performed by using isotopically labeled proteins or by exchanging amino acids via site directed mutagenesis.

Isotopic labeling shifts the stretching frequency, ν of the labeled group due to the increased reduced mass μ, as follows:

$$\nu = \frac{1}{2\pi}\sqrt{\frac{k}{\mu}},$$

where k is the force constant. Chemical synthesis can be used to isotopically label prosthetic groups, like retinal [36], or nucleotides, like GTP [18,37,38]. Biosynthetic incorporation of isotopically labeled amino acids is used for labeling all amino acids of one kind within a protein [39,40]. Fig. 6A shows schematically the effect of isotopic labeling of Thr35 in Ras. All corresponding vibrations will red-shift due to the higher mass. This example is also used below, where the original data from the measurements are shown.

Furthermore, site-directed exchange of an amino acid by mutagenesis eliminates the absorption band of the exchanged group (Fig. 6B). The wildtype (wt) spectrum includes the bands that correspond to Thr35. The mutant is missing this group, and thus, the corresponding absorption bands do not appear. Instead, bands that correspond to the introduced group might appear. Mutation of an amino acid can change the structure of the protein to a greater or lesser degree. The similarity between the wt and mutant spectra indicates whether the mutation is invasive. In the case of Ras, most mutants in the switch I region (residues 32–38, including Thr35 mutants) lead to a change in the whole loop; thus, band assignment by site-directed mutagenesis is not possible. Nevertheless, the method was very successful, for example, for assigning the bands in bR [10]. Isotopic labeling offers the advantage of marking the molecular group without disrupting the structure. Currently, chemical synthesis of a protein allows site-directed isotopic labeling, and this may become the method of the future [41–43]. Non-disruptive site-directed modifications can also be performed with amber codon suppression technology, which uses non-natural amino acids [44].

2.7. Attenuated total reflection (ATR)-FTIR

For ATR (Fig. 2B), the IR light is reflected at the interface between the sample and the internal reflection element (IRE, a crystal with high refractive index, most commonly made of diamond, ZnSe, Si, or Ge). In this process, an evanescent wave penetrates into the sample. The depth D, where the electric field of this wave is reduced to 37%, can be calculated as follows:

$$D = \frac{\lambda}{2\pi n_C\sqrt{\sin^2\alpha - \left(\frac{n_S}{n_C}\right)^2}},$$

where λ is the wavelength, n_S is the refractive index of the sample, n_C the refractive index of the crystal, and α is the angle of incidence.

In most cases, D is in the low μm range, and molecules which are close to the surface contribute strongest to the absorption. Due to the limited depth of penetration of the evanescent field the limited overall effective thickness of the measured sample is preventing total absorption due to the absorbance of water. Under optimal measurement conditions even monolayers (e.g., of lipids and functional proteins and their action) can be investigated.

Furthermore, proteins can be immobilized by anchoring them to a substrate attached to the ATR-crystal. Various techniques for protein immobilization are available; among them is covalent

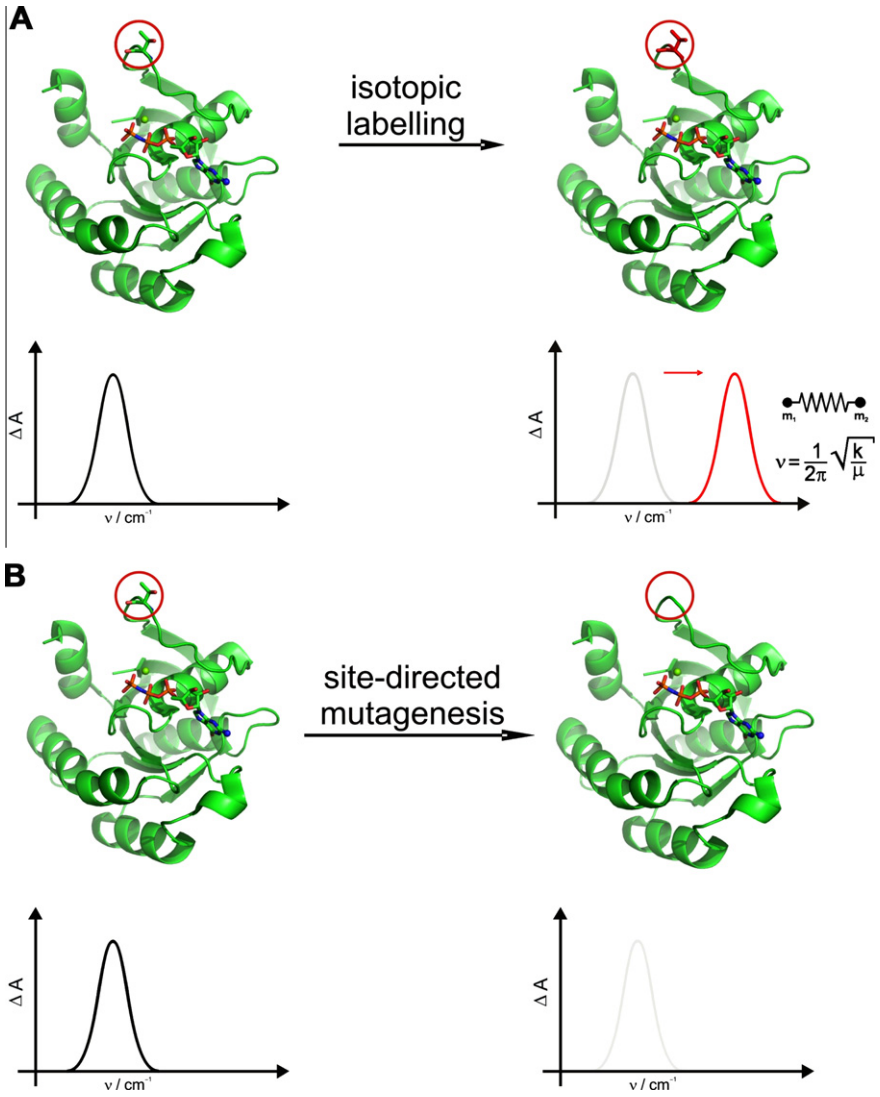

Fig. 6. Band assignment. (A) Isotopic labeling. One amino acid of the protein is isotopically labeled; e.g., by ^{15}N, ^{13}C, or ^{2}H. Due to the increased mass, the corresponding vibrations are shifted to lower wavenumbers. (B) Site directed mutagenesis. One amino acid is substituted with a different amino acid; the corresponding vibrations vanish in the spectrum of the mutant.

attachment via cysteine residues or anchoring of the protein by lipid anchors to model membranes [8,45]. In contrast to transmission experiments, with ATR cells the sample preparation can be monitored within the spectrometer. This facilitates the extraction of quantitative information such as surface concentration, structural information and the molecular orientation of the immobilized sample.

Further, difference spectroscopic investigation of an immobilized protein can be triggered additional to the usual trigger techniques describes above by simply alternating the buffer composition. Structural changes of the protein due to added ligands or varying pH or ionic strength can be monitored in atomic detail as previously described. In addition protein–protein-interaction studies are possible.

Depending on the sample thickness d compared to the penetration depth of the evanescent field the results can be interpreted via the thin film – ($d < D/10$), or the thick film ($d > D$) approximation [5,6]. As the field intensities of the evanescent wave depends on the refractive indices of IRE, sample, and solvent (medium) in thick film one has to know the refractive index of the sample to analyze and interpret the spectrum of the sample. This circular causality complicates the spectra interpretation. This can be overcome using the thin film approximation in combination with the weak absorber approximation [46] which allows spectra interpretation of thin sample layers ($d < D/10$) with unknown refractive indices.

Difference spectroscopic investigations of proteins by ATR are mostly done by thick films of hydrated proteins, which are excited either by ligand addition [47] or by light flashes [48]. In the last decade SEIRA (Surface Enhanced Infrared Absorption) spectroscopy of protein-monolayers covalently immobilized on gold-coated Silicon IREs [3,15] was introduced. In SEIRA experiments a rough island like gold surface builds up a strong near field in which the absorbance is increased by a factor of 10–100 compared to non surface enhanced setups [3,49,50]. However, the enhancement depends on the relative orientation of the transition dipole moment and the spectral region. This can change the spectral signature and conformational and orientational changes are difficult to distinguish. Further, the gold film absorbs, depending on its thickness, a lot of the IR intensity, which decreases the signal/noise (S/N) ratio.

In contrast in ATR-experiments with IREs made of germanium, which is due to the high refractive index of 4 an ideal ATR-material, the signal can be increased by multiple internal reflections by a

factor of 10–25 easily, leading to signal intensities similar to intensities obtained by SEIRA experiments with one reflection. Both orientational- and difference spectroscopic information can be obtained from protein-monolayers [51]. Since the thin-film approximation is valid here, quantitative information can be obtained. In the following we describe the first time resolved FTIR investigation of an enzymatic reaction of a protein anchored at a single lipid bilayer using this technique.

3. Time-resolved FTIR studies of GTPases

3.1. The GTPase Ras

In a eukaryotic cell, about 150 different small GTPases regulate a large variety of processes [52] by acting as molecular switches. For most GTPases a GTP bound "on" state and a GDP bound "off" state exist. The switch to the "off" state is accomplished by GTP hydrolysis. GTP hydrolysis in water has a half life of several days, but GTP bound to Ras has a half life of minutes. In addition, GTPase activating proteins (GAP) further accelerate hydrolysis by about 10^5 fold. In oncogenic Ras, this catalysis is inhibited, and the downstream signal is no longer down-regulated. This is a major event in the transformation of a cell into a cancer cell. The GTPase can be reactivated by exchanging GDP with GTP. This process is accelerated with guanine nucleotide exchange factors (GEF).

Ras is a prototype GTPase in the superfamily of small GTPases, and it is the best-studied member [53]. Ras exists in three isoforms (H-, N,- and K-Ras) with nearly identical G-domains but variable C-termini; the C-terminus is posttranslationally modified by, depending on the isoform, one to three lipid anchors that control membrane targeting. Recent investigations on membrane anchored Ras have suggested that membrane anchoring plays an active role in effector interactions and in the switching mechanism [54]. However, most biophysical studies were performed with a truncated form of the Ras protein (H-Ras 1–166) without the anchor.

GTPase interactions with their GTP ligands can be studied with time-resolved FTIR spectroscopy and caged GTP as the photolabile trigger [19,55]. This approach demonstrated that, upon GTP binding to Ras, a specific charge distribution was induced in GTP that reduced the free activation energy [56]. This catalyzed GTP hydrolysis. In addition, protein–protein interactions, e.g., the activation of Ras by GAP protein, was studied [57,58] with FTIR spectroscopy. FTIR assays can allow label-free screening for drug-protein interactions [59].

3.2. The reaction mechanism of Ras at the atomic level

In the following examples, we demonstrate how the techniques introduced above led to information on the reaction mechanisms of Ras. Fig. 7A shows the assignment of a marker band for the "off" to "on" transition in Ras. The band at 1689 cm^{-1} (yellow) was shifted when threonine was labeled with ^{13}C; therefore, 1689 cm^{-1} was assigned to the Thr35 of Ras. Thr35 is within the switch-I region (residues 32–38) [52] of Ras, which exhibits a conformational change during the "off" to "on" reaction. Fig. 7B shows the time resolved absorbance changes during this switch with the Thr35 band marked in yellow. The switch-I movement was observed with a rate constant of 5 s^{-1} at 260 K. The structural models of the "on" state (pdb 5p21) vs. the "off" state (pdb 1X1S) shows that the carbonyl group of the Thr35 backbone changed from a solvent-exposed state to a protein-buried state in the switching process. In the "on" state, hydrogen bonding is weaker, and thus, this band is found at higher wavenumbers.

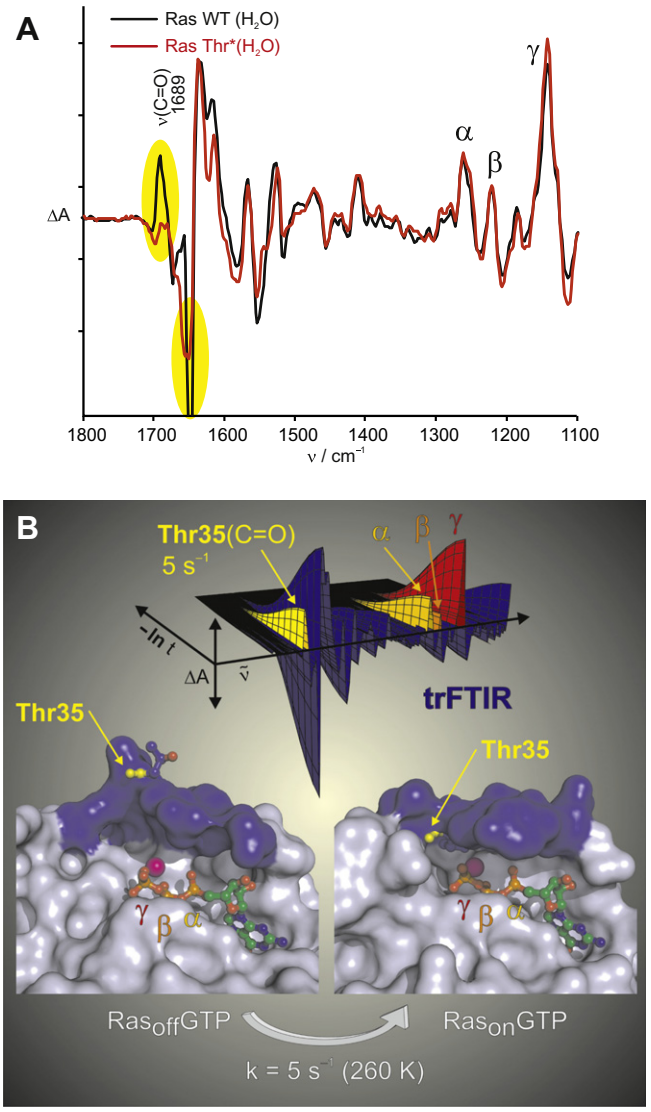

Fig. 7. Assignment of a marker band for the switching reaction. (A) Amplitude spectra of the switching reactions for unlabeled Ras (black), and Ras labeled with $^{13}C_4{}^{15}N$-threonine (red). The band at 1689 cm^{-1} is assigned to the carbonyl stretching vibration of unlabeled Thr35. This band is shifted in the labeled spectrum. Due to an overlap of the shifted band with a strong negative band this leads to a reduced intensity of the negative band only. (B) Time resolved absorbance changes in the mid-IR range during the switching reaction. In addition to the marker band of Thr35, many other vibrations are observed, including the vibrations that correspond to the α-, β-, and γ- phosphates of GTP; This indicates an environmental change within the binding pocket. The carbonyl group of Thr35 is shown in yellow in the structural models. In the "off" state, the group is solvent-exposed; in the "on" state, it is buried in a more hydrophobic environment [55].

Similarly, many bands of Ras were assigned, which led to a detailed understanding of the GAP catalyzed GTPase reaction. Fig. 8 shows the time course of three marker bands in this reaction [58]. The global fit was performed with three exponential functions. In the first step after decaging (k_1), the GTPase changed into its "on" conformation, evidenced by the Thr35 band (Fig. 8A). In the next step (k_2), the catalytic arginine finger moved into the binding pocket (Fig. 8B), which initiated bond breakage. This step was entropy driven, because ordered water molecules were pushed out of the binding pocket into the bulk solution [58]. Bond breakage produced a protein-bound phosphate (Fig. 8C). The FTIR spectrum showed that this P_i was doubly protonated ($H_2PO_4^-$) and hydrogen bonded to the GDP [57]. In the last step (k_3), the

arginine left the binding pocket, the phosphate was released into the bulk solution, and the Ras returned to the "off" state.

4. Tr-FTIR studies of GTPases at a membrane

In this experiment, Ras was immobilized at a SSLB with a semi-synthetic lipid anchor [8]. The SSLB was thoroughly characterized to be a single bilayer: Fig. 9A shows the difference spectrum obtained from the bilayer preparation. Bands from POPC are facing upwards. Since the POPC displaces water molecules out of the probed volume negative water bands are present (marked in blue). By means of the intensities of the CH_2 stretching vibrations of the lipid (marked in yellow) we calculated the surface density of the lipid to be 450 ± 60 pmol/cm^2 as expected for a bilayer. An almost identical surface density of 460 pmol/cm^2 was obtained by preparation of a POPC bilayer by the Langmuir–Blodgett technique [60]. From the difference spectrum of the protein immobilization (Fig. 9B) we obtained in the same way using the intensity of the amide II band (green) the surface density for Ras as 13 ± 2 pmol/cm^2, which corresponds to roughly 80% coverage of the monolayer.

As an independent method for the characterization we used atomic force microscopy (AFM). The topography of the SSLB is very similar to the topography of an empty crystal (Supplementary Fig. 2) indicating a very thin and uniform film. We further prepared an incomplete SSLB as shown in Fig. 9C. The topography shows patches of a bilayer surrounded by empty surfaces. The step size between covered and uncovered areas is 4 nm in accordance with a POPC bilayer [61]. More details on the membrane characterization including the determination of order parameters, experimental conditions and calculations are given as Supplementary material.

In the Ras anchored to the membrane (Fig. 10A), GDP was exchanged by GTP and subsequently the hydrolysis reaction was observed with time-resolved FTIR. This showed a rate of $6.5 \cdot 10^{-5}$ s^{-1}, which was very similar to the rate of $5.0 \cdot 10^{-5}$ s^{-1} observed for truncated Ras in solution (both at 293 K, Fig. 10B). The difference spectra between Ras GTP and Ras GDP in solution and at the membrane are shown in Fig. 10C. Interestingly, these difference spectra were very similar. The implications of this result are discussed in the following section.

4.1. Spectral effects of membrane anchoring

The positions of all difference bands (Fig. 10C) were mostly the same, e.g. the "on"-state marker-band of Thr35 at 1690 cm^{-1}. The visible differences are mainly some band intensities, which can be explained by alterations in the experimental conditions: Experiments with the truncated Ras were performed in a closed cuvette. Thus, all reaction products were observed. On the other hand, experiments with the membrane anchored Ras were performed in a flow-through cuvette, and the products that were not bound to the protein were washed away. This is nicely illustrated with the released P_i band at 1078 cm^{-1} [62]; this band was observed in the closed cuvette but not in the ATR-FTIR experiment. The second obvious difference was the lower intensity around 1650 cm^{-1}

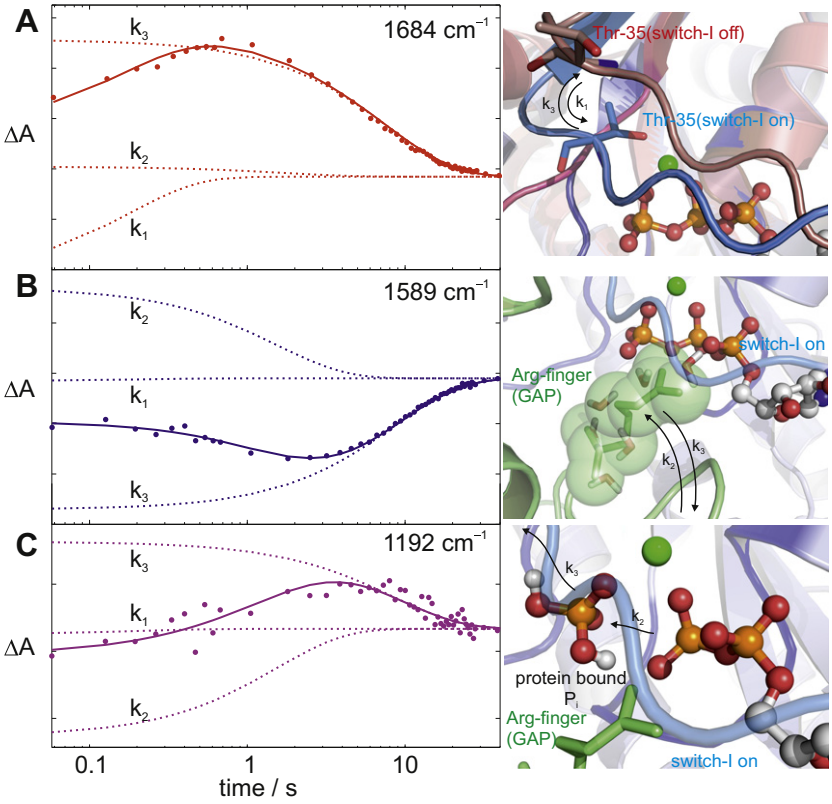

Fig. 8. Time-dependent absorbance changes during the GTPase reaction of the Ras·GAP protein–protein complex. (A) Time-dependent absorbance changes of the Thr35 marker band (in D_2O) for switch I in Ras. The three exponentials in the global fit are shown as dotted lines. The band appears with rate 1, which indicates that this rate represents the conformational change from "off" to "on". This movement is shown on the right side as the change from the red "off" to the blue "on" conformation of switch 1. The absorbance disappears with rate 3; this indicates that this rate represents the reverse conformational change from "on" to "off". (B) Time-dependent absorbance changes of a marker band (in D_2O) for the arginine of GAP in a water environment. The three exponentials in global fit are shown as dotted lines. The band decreases with rate 2; this indicates the movement of the arginine into the binding pocket. The arginine (green spheres) replaces ordered water molecules in the binding pocket, which increases the entropy of activation [58]. The absorbance increases with rate 3; this indicates the change back toward the water environment. (C) Time-dependent absorbance changes of a marker band (in D_2O) for the protein-bound P_i. This intermediate appears with bond breakage (k_2) and disappears with P_i-release (k_3) [57].

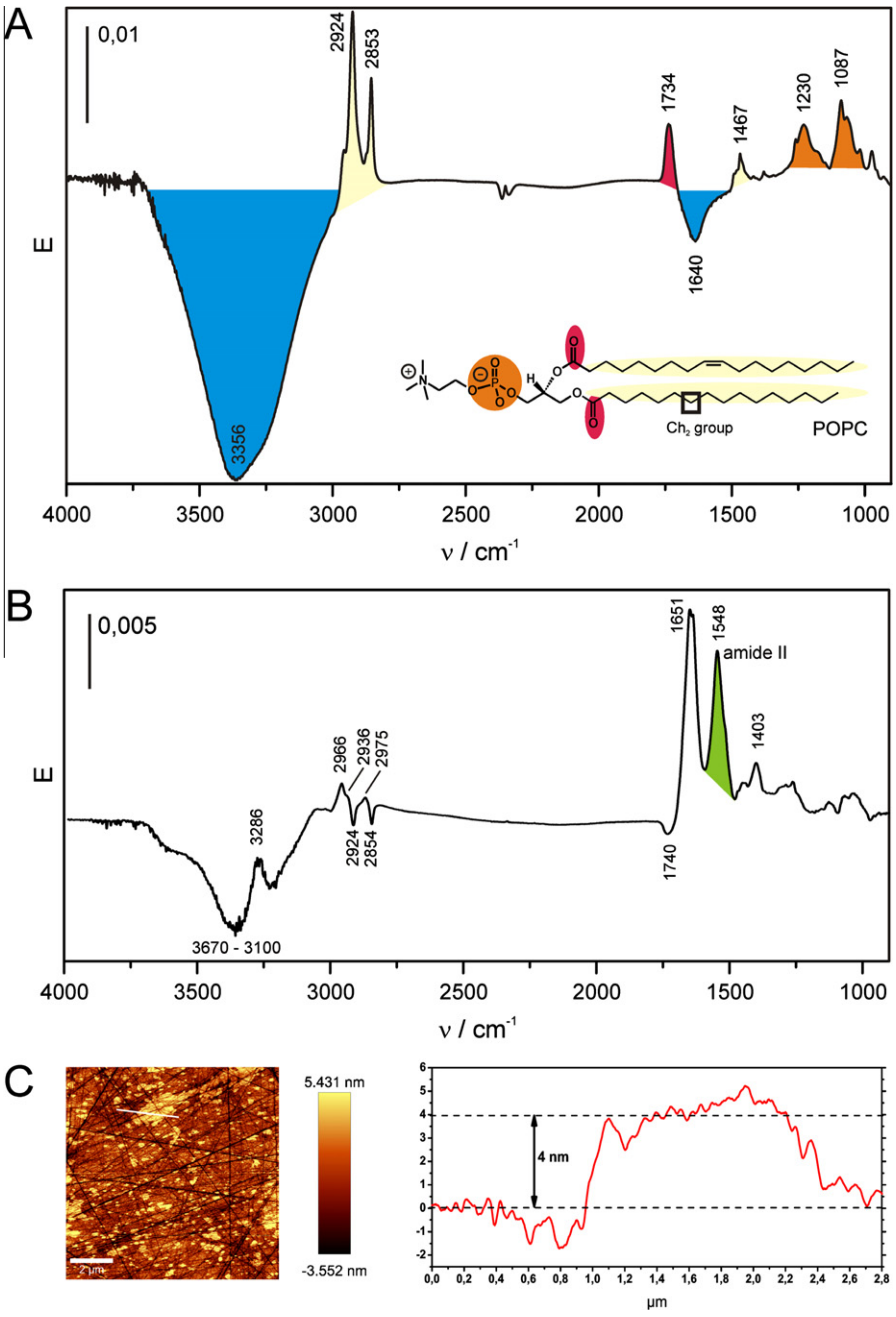

Fig. 9. Characterization of the SSLB and the bound Ras protein. (A) Difference spectrum of the bilayer formation. Bands facing upwards are due to the POPC bilayer, bands facing downwards are from the displaced water. The functional groups of POPC and their corresponding absorption bands are color coded. The intensity of the bands of the CH_2 groups is used for the calculation of the surface density, which corresponds to a single bilayer (see text and Supplementary information). (B) Difference spectrum of the protein immobilization. Bands facing upwards are due to the lipidated protein and bands facing downward are due to the displaced water and perturbed POPC molecules. The amide II band at 1548 cm^{-1} (green) was used for the calculation of the surface density of the Ras protein which again corresponds to a single protein layer with about 80% surface coverage. (C) The topography of a 18% complete SSLB measured by AFM. The cross section (according to the white line on the left) on the right side shows that the patches correspond to single bilayers with a height of ~4 nm. The scratches are from the polishing procedure. For more details see text and Supplementary information.

in the closed cuvette. This spectral region is always problematic, due to the strong absorbances of water and the amide I mode, which lead to a low transmittance, and thus, a bad S/N ratio. In the ATR-experiments, the transmittance in that region was much higher.

4.2. The role of the anchoring

Another reason for the stronger amide I signal could be a change in orientation of the protein. The G-domain orientation with respect to the plane of the plasma membrane was thought to be an important factor in regulating Ras interactions with effectors [54]. FRET-experiments with Ras linked to GFP-derivates on whole cells as well as molecular dynamics simulations of Ras in a membrane environment point in this direction [63,64]; however, there is no direct biophysical measurement of this orientation change reported. In future experiments, this could be elucidated on our setup with polarized ATR measurements. In our measurements there were negligible changes in the C=O stretching region (~1740 cm^{-1}) during the hydrolysis reaction. This indicated, that no large change of interaction of cationic residues e.g. lysines or arginines with the CO – ester groups of the lipids occurred,

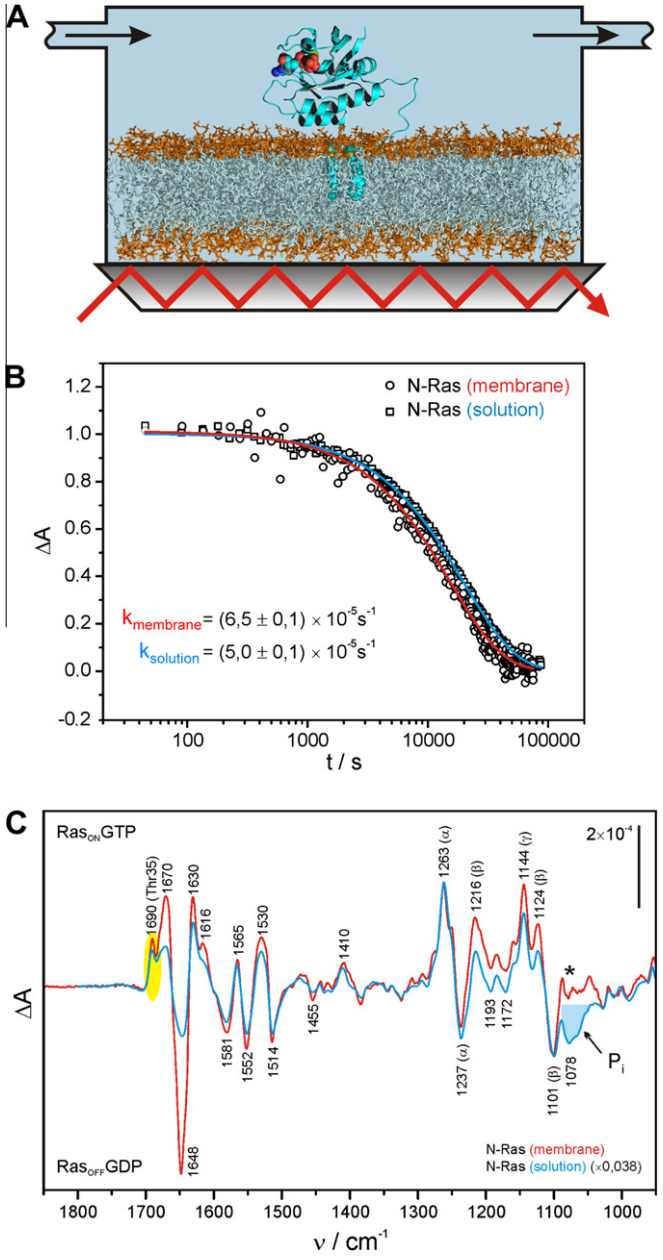

Fig. 10. Time-resolved FTIR spectroscopy of a membrane-bound protein. (A) Schematic representation of the setup. A SSLB is formed on top of a germanium ATR crystal. N-Ras is immobilized with lipid anchors. Subsequently, nucleotide exchange, protein interactions, and other reactions can be investigated. (B) Time course of the GTPase reaction of N-Ras in solution (blue) and bound to a membrane (red). (C) Spectra of the hydrolysis reaction. Bands facing upwards represent the GTP "on" state; bands facing downwards represent the GDP "off" state. Both the kinetics and spectra indicate that the membrane made no major contribution to the GTPase reaction.

which speaks against an orientation change of the protein upon changing the nucleotide from GTP to GDP. On the one hand this result showed that the membrane-anchoring did not lead to drastic changes of the nucleotide binding properties and the intrinsic hydrolysis reaction of Ras. This implies that the large amount of data generated for truncated Ras in solution measurements is likely to be valid also for Ras in its more native membrane-bound situation. On the other hand it is possible that other lipids e.g. charged lipids or raft-mixtures have an impact on the Ras activity.

Summing up, our results did not suggest any additional functions of the anchor beyond membrane targeting. Besides providing a more physiological environment, the immobilization of proteins at membranes enables an additional manifold of experimental possibilities.

4.3. Experimental capabilities of FTIR of immobilized proteins

A mayor advantage of the ATR-technique is the better accessibility of the immobilized proteins compared to protein solutions in closed cuvettes. This enables the investigation of the influence of external factors, e.g. ligands, interacting proteins, pH, and ionic strength, successively on the same sample: First, the sample-accessibility in the flow-through system can be used for varying ligand or small molecule concentrations in a titration experiment and simultaneously monitoring the conformational changes of the protein which allows the extraction of binding affinities and the localization of the binding site. Second, experiments to study protein–protein interactions similar to surface plasmon resonance experiments can be realized – first experiments with immobilized Ras and the Ras binding domain of the effector Nore1A confirmed comparability with standard methods in terms of the determined K_D. Additional information, e.g. on the protein conformation, is obtained from the FTIR spectrum. Third, investigating reactions of immobilized proteins by triggering the reaction through flushing the system with ligands is possible. This should allow measuring e.g. the GEF catalyzed nucleotide exchange reaction in a more native membrane environment with FTIR for the first time. Fourth, another experimental advantage of the open geometry of the ATR-cell is the easy combinability with other techniques, e.g. atomic force microscopy (AFM) or fluorescence spectroscopy. Two techniques can be used to measure simultaneously the same sample. This aspect could be used to analyze the recently found feature of plasma membrane bound Ras to build up nanoclusters of a few Ras molecules [65]. This clustering and its localization to different membrane regions depend on the isoform and the activation state of Ras. The cause of this clustering, which seems to have a big effect on Ras-signaling, is still a matter of debate and a biophysical explanation is missing.

4.4. Conclusion

In summary, time-resolved FTIR difference spectroscopy is a powerful tool for monitoring protein–ligand or protein–protein interactions. FTIR is complementary to X-ray or NMR analysis. The latter provide three dimensional structural models of proteins, and the former delivers information on H-bonding, protonation states, charge distributions, and time dependencies of protein reactions and protein interactions.

5. Experimental procedures

5.1. Materials

We purchased 1-palmitoyl-2-oleoyl-sn-glycero-3-phosphocholine (POPC) from Lipoid (Lipoid GmbH, Ludwigshafen, Germany). Lipid solutions were prepared at a concentration of about 32 mM in chloroform. Lipid vesicle solutions were prepared in buffer (10 mM Tris/HCl pH 7.4, 5 mM $MgCl_2$). A 9.5 g/l protein stock solution was used for the injection of N-Ras protein onto the binding buffer solution (20 mM Tris/HCl pH 7.4, 5 mM $MgCl_2$, 1 mM DTT, 0.1 mM GDP) that bathed the adsorbed POPC model membrane. The nucleotide exchange and hydrolysis reactions were performed in buffer H (50 mM MES, 100 mM NaCl, 1 mM DTT, pH 6.5) with the addition of 5 mM $MgCl_2$, 10 mM EDTA, and 0.1 mM GTP.

The measurements were performed with a vertical ATR multireflection unit, (Specac, Orpington, UK) mounted in a Vertex 80 V spectrometer (BrukerOptics, Ettlingen, Germany). The internal reflection element (IRE) was a 52 mm × 20 mm × 2 mm trapezoidal germanium ATR plate with an aperture angle of 45°. In this experiment, only one side of the IRE was used, which resulted in 13 active reflections.

The semisynthetic N-Ras protein used in these experiments was prepared as described elsewhere [8,66–69]. N-Ras1–180His was used for comparison; it was expressed as described for N-Ras without the His-Tag [70]. The purification was carried out with immobilized metal ion affinity chromatography (IMAC) and size exclusion chromatography.

5.2. Preparation of the ATR crystals

Prior to each measurement, both sides of the germanium IRE were polished for 5 min by machine (Logitech CP50, Logitech, Old Kilpatrick, Scotland) with a diamond polishing suspension (0.1 μm, Logitech) on a hard cloth (Microtex 500 HC-W, Logitech) that rotated at 40 rpm. After rinsing the IRE with Millipore water, the hydrophilic character of the IRE surfaces were attained by dipping the IRE for 10 min into a concentrated sulfuric acid solution, followed by rinsing, and then drying under a nitrogen gas flow. In order to further enhance the hydrophilic character of the IRE and to remove small traces of organic compounds, we finally treated the IRE for 5 min with air plasma (Harrick Sci. Corp., Pleasantville, NY, USA).

5.3. Bilayer preparation and protein Immobilization

The solid supported lipid bilayer (SSLB) was prepared by spreading vesicles onto hydrophilic IRE surfaces. After SSLB preparation and subsequent washing steps, the lipid-anchored N-Ras was added to the circulating flow-through system. This resulted in a slow immobilization of the protein. Both procedures were described in detail previously [8].

5.4. Nucleotide exchange and hydrolysis measurements

Ras was immobilized in a GDP-bound form. In order to investigate the intrinsic hydrolysis reaction from GTP to GDP, the nucleotide had to be exchanged. This was performed in a series of incubations with four different buffers. Prior to the nucleotide exchange, the binding buffer in the cuvette was replaced with the hydrolysis buffer (buffer H; Section 5.1). In Step 1, the system was washed with buffer H supplemented with 5 mM $MgCl_2$. After 10 min, all the binding buffer in the cuvette was replaced, and a reference spectra was recorded. In Step 2, the surface was incubated with buffer H supplemented with 10 mM EDTA + 0.1 mM GTP for 30 min. This lowered the nucleotide affinity of Ras, because Mg^{2+} was chelated with EDTA [71]. In the presence of excess GTP, this caused the displacement of GDP by GTP. In Step 3, the cuvette was flushed with buffer H supplemented with 5 mM $MgCl_2$, 0.1 mM GTP for 3 min. This ensured strong binding of the residual GTP. In Step 4, the buffer was exchanged with the same buffer used for the reference spectra in Step 1, and the hydrolysis kinetics were measured.

5.5. ATR measurements and spectra analyses

Measurements with the ATR unit and the Aquaspec cell were performed at 293 K with a spectral resolution of 2 cm^{-1} and a scanner velocity of 80 kHz; scans were performed in a double-sided forward–backward mode. The resulting interferograms were apodized with the Blackman-Harris three-term function, and with a zero filling factor of 4. The measurement parameters for the closed transmission cuvette setup were described previously [56].

The hydrolysis kinetics was extracted from the 3D spectra by subtracting the extinction values of nearby difference bands, as described previously [56]. This method eliminated baseline drifts. Difference absorbance kinetics of α-GTP- and α-GDP-bands (1263 cm^{-1} and 1237 cm^{-1}, respectively) were used in solution measurements. In the ATR measurements, the α-Phosphate region was obscured by a spacer artifact of the cuvette; thus, the kinetics were extracted as the absorbance of the γ-GTP band (1144 cm^{-1}) corrected with a linear baseline from 1170 cm^{-1} to 1116 cm^{-1}.

The hydrolysis spectra of Ras in solution were extracted by global fitting of the 3D spectrum, as described above. The hydrolysis spectra of membrane-bound Ras were extracted from a set of four ATR experiments by MCR with alternating least squares fitting [72]. The measurement artifacts (e.g., baseline drifts, spacer bands, and water vapor bands) were independent from the exponentially decaying hydrolysis signal; this allowed extraction of a hydrolysis spectrum from the difference absorbances of a monolayer. The difference absorbances in the monolayer were >20 times lower than those from transmission experiments.

5.6. Hydrolysis measurements in solution

The hydrolysis reactions were compared between the membrane-bound Ras and the truncated Ras in solution. The solution experiment (Fig. 10C) used N-Ras1–181His loaded with caged-GTP in a closed transmission cuvette, as described in detail previously [56]. The hydrolysis kinetics (Fig. 10B) were measured with GTP-loaded N-Ras1–181His which was injected directly after GTP loading as a 0.7 mM solution in an Aquaspec flow cell (Micro-Biolytics, Esslingen, Germany). Ras was loaded with GTP via the EDTA method [71], followed by a 1 min gel filtration step (Zeba Spin Desalting Columns, Pierce Biotechnology, Rockford, US), in which the buffer was exchanged to buffer H supplemented with 5 mM $MgCl_2$. The Aquaspec cell was mounted in a Vertex 80 V spectrometer (BrukerOptics, Ettlingen, Germany) and the temperature was maintained constant at 293 K during the entire measurement.

Acknowledgments

We thank Herbert Waldmann and Gemma Triola for the semisynthetic N-Ras protein; Laven Mavarani for performing the AFM measurements; Philipp Pinkerneil for the reference spectra and preparation of N-Ras1–181His; and Till Rudack for help with one of the Figures. We gratefully acknowledge support from the SFB 642 (DFG) and the CVM (co-financed by the EU and the state North Rhine-Westphalia).

Appendix A. Supplementary data

Supplementary data associated with this article can be found, in the online version, at doi:10.1016/j.chemphys.2011.08.007.

References

[1] A. Barth, P.I. Haris, Biological and Biomedical Infrared Spectroscopy, IOS Press BV, Amsterdam, 2009.
[2] F. Siebert, P. Hildebrandt, Vibrational Spectroscopy in Life Science, Wiley-VCH, Weinheim, 2008.
[3] K. Ataka, T. Kottke, J. Heberle, Angew. Chem. Int. Ed. 49 (2010) 5416.
[4] I. Radu, M. Schleeger, M. Nack, J. Heberle, Aust. J. Chem. 64 (2011) 9.
[5] U.P. Fringeli, D. Baurecht, M. Siam, G. Reiter, M. Schwarzott, T. Burgi, P. Bruesch, Handbook of Thin Film Materials, vol. 2, Academic Press, San Diego, USA, 2002, pp. 191–229.
[6] N.J. Harrick, Appl. Spectrosc. 41 (1987) 1.
[7] E. Kauffmann, N.C. Darnton, R.H. Austin, C. Batt, K. Gerwert, Proc. Natl. Acad. Sci. USA 98 (2001) 6646.

[8] J. Güldenhaupt, Y. Adigüzel, J. Kuhlmann, H. Waldmann, C. Kötting, K. Gerwert, FEBS J. 275 (2008) 5910.
[9] E. Goormaghtigh, R. Gasper, A. Benard, A. Goldsztein, V. Raussens, Biochim. Biophys. Acta Proteins Proteomics 1794 (2009) 1332.
[10] K. Gerwert, G. Souvignier, B. Hess, Proc. Natl. Acad. Sci. USA 87 (1990) 9774.
[11] K. Gerwert, Ber. Bunsen Ges. 92 (1988) 978.
[12] A. Remy, K. Gerwert, Nat. Struct. Biol. 10 (2003) 637.
[13] K. Ataka, B. Richter, J. Heberle, J. Phys. Chem. B 110 (2006) 9339.
[14] D. Moss, E. Nabedryk, J. Breton, W. Mantele, Eur. J. Biochem. 187 (1990) 565.
[15] I. Zebger, D. Millo, P. Hildebrandt, M.E. Pandelia, W. Lubitz, Angew. Chem. Int. Ed. 50 (2011) 2632.
[16] A.P. Pelliccioli, J. Wirz, Photochem. Photobiol. Sci. 1 (2002) 441.
[17] J.A. McCray, D.R. Trentham, Ann. Rev. Biophys. Biophys. Chem. 18 (1989) 239.
[18] V. Cepus, C. Ulbrich, C. Allin, A. Troullier, K. Gerwert, Methods Enzymol. 291 (1998) 223.
[19] C. Völlmecke, C. Kötting, K. Gerwert, M. Lubben, FEBS J. 276 (2009) 6172.
[20] Q. Cheng, M.G. Steinmetz, V. Jayaraman, J. Am. Chem. Soc. 124 (2002) 7676.
[21] A. Barth, J.E.T. Corrie, Biophys. J. 83 (2002) 2864.
[22] J. Walker, G.P. Reid, J.A. McCray, D.R. Trentham, J. Am. Chem. Soc. 110 (1988) 7170.
[23] C.-H. Park, R.S. Givens, J. Am. Chem. Soc. 119 (1997) 2453.
[24] M. Schleeger, C. Wagner, M.J. Vellekoop, B. Lendl, J. Heberle, Anal. Bioanal. Chem. 394 (2009) 1869.
[25] R. Rammelsberg, S. Boulas, H. Chorongiewski, K. Gerwert, Vib. Spectrosc. 19 (1999) 143.
[26] R.A. Palmer, J.L. Chao, R.M. Dittmar, V.G. Gregoriou, S.E. Plunkett, Appl. Spectrosc. 47 (1993) 1297.
[27] R.A. Palmer, C.J. Manning, J.L. Chao, I. Noda, A.E. Dowrey, C. Marcott, Appl. Spectrosc. 45 (1991) 12.
[28] O. Weidlich, F. Siebert, Appl. Spectrosc. 47 (1993) 1394.
[29] W. Uhmann, A. Becker, C. Taran, F. Siebert, Appl. Spectrosc. 45 (1991) 390.
[30] B. Hessling, J. Herbst, R. Rammelsberg, K. Gerwert, Biophys. J. 73 (1997) 2071.
[31] B. Hessling, G. Souvignier, K. Gerwert, Biophys. J. 65 (1993) 1929.
[32] C.R. Cantor, P.R. Schimmel, Biophys. Chem. Pt. 1: Conform. Biol. Macromol. (1980).
[33] A. Fersht, Enzymes: Structures and Reaction Mechanisms, W.H. Freeman, 1983.
[34] J.I. Steinfeld, J.S. Francisco, W.L. Hase, Chemical Kinetics Dynamics, second ed., Prentice Hall, 1999.
[35] L. Blanchet, C. Ruckebusch, A. Mezzetti, J.P. Huvenne, A. de Juan, J. Phys. Chem. B 113 (2009) 6031.
[36] J. Lugtenburg, R.A. Mathies, R.G. Griffin, J. Herzfeld, Trends Biochem. Sci. 13 (1988) 388.
[37] C. Allin, M.R. Ahmadian, A. Wittinghofer, K. Gerwert, Proc. Natl. Acad. Sci. USA 98 (2001) 7754.
[38] C. Allin, K. Gerwert, Biochemistry 40 (2001) 3037.
[39] M. Engelhard, K. Gerwert, B. Hess, F. Siebert, Biochemistry 24 (1985) 400.
[40] B. Warscheid, S. Brucker, A. Kallenbach, H.E. Meyer, K. Gerwert, C. Kötting, Vib. Spectrosc. 48 (2008) 28.
[41] W.B. Fischer, S. Sonar, T. Marti, H.G. Khorana, K.J. Rothschild, Biochemistry 33 (1994) 12757.
[42] C.F.W. Becker, C.L. Hunter, R. Seidel, S.B.H. Kent, R.S. Goody, M. Engelhard, Proc. Natl Acad. Sci. USA 100 (2003) 5075.
[43] S. Tremmel, M. Beyermann, H. Oschkinat, M. Bienert, D. Naumann, H. Fabian, Angew. Chem. Int. Ed. 44 (2005) 4631.
[44] S.X. Ye, E. Zaitseva, G. Caltabiano, G.F.X. Schertler, T.P. Sakmar, X. Deupi, R. Vogel, Nature 464 (2010) 1386.
[45] K. Elfrink, J. Ollesch, J. Stohr, D. Willbold, D. Riesner, K. Gerwert, Proc. Natl. Acad. Sci. USA 105 (2008) 10815.
[46] N.J. Harrick, K.H. Beckmann, J. Electrochem. Soc. 115 (1968). C61-&.
[47] E. Padros, M. Granell, X. Leon, G. Leblanc, V.A. Lorenz-Fonfria, Proc. Natl. Acad. Sci. USA 107 (2010) 22078.
[48] C. Zscherp, R. Schlesinger, J. Tittor, D. Oesterhelt, J. Heberle, Proc. Natl. Acad. Sci. USA 96 (1999) 5498.
[49] K. Ataka, J. Heberle, Anal. Bioanal. Chem. 388 (2007) 47.
[50] M. Osawa, Top. Appl. Phys. 81 (2001) 163.
[51] N. Hassler, D. Baurecht, G. Reiter, U.P. Fringeli, J. Phys. Chem. C 115 (2011) 1064.
[52] I.R. Vetter, A. Wittinghofer, Science 294 (2001) 1299.
[53] A.D. Cox, C.J. Der, Small GTPases 1 (2010) 2.
[54] D. Abankwa, M. Hanzal-Bayer, N. Ariotti, S.J. Plowman, A.A. Gorfe, R.G. Parton, J.A. McCammon, J.F. Hancock, EMBO J. 27 (2008) 727.
[55] C. Kötting, A. Kallenbaczh, Y. Suveyzdis, C. Eichholz, K. Gerwert, ChemBioChem 8 (2007) 781.
[56] C. Kötting, K. Gerwert, Chem. Phys. 307 (2004) 227.
[57] C. Kötting, M. Blessenohl, Y. Suveyzdis, R. Goody, A. Wittinghofer, K. Gerwert, Proc. Natl. Acad. Sci. USA 103 (2006) 13911.
[58] C. Kötting, A. Kallenbach, Y. Suveyzdis, A. Wittinghofer, K. Gerwert, Proc. Natl. Acad. Sci. USA 105 (2008) 6260.
[59] C. Kötting, Y. Suveyzdis, R.S. Bojja, N. Metzler-Nolte, K. Gerwert, Appl. Spectrosc. 64 (2010) 967.
[60] S.A. Tatulian, Biochemistry 42 (2003) 11898.
[61] R. Richter, A. Mukhopadhyay, A. Brisson, Biophys. J. 85 (2003) 3035.
[62] M. Klähn, G. Mathias, C. Kötting, M. Nonella, J. Schlitter, K. Gerwert, P. Tavan, J. Phys. Chem. A 108 (2004) 6186.
[63] D. Abankwa, A.A. Gorfe, K. Inder, J.F. Hancock, Proc. Natl. Acad. Sci. USA 107 (2010) 1130.
[64] A.A. Gorfe, M. Hanzal-Bayer, D. Abankwa, J.F. Hancock, J.A. McCammon, J. Med. Chem. 50 (2007) 674.
[65] Y.I. Henis, J.F. Hancock, I.A. Prior, Mol. Membr. Biol. 26 (2009) 80.
[66] L. Brunsveld, J. Kuhlmann, K. Alexandrov, A. Wittinghofer, R.S. Goody, H. Waldmann, Angew. Chem. Int. Ed. 45 (2006) 6622.
[67] K. Kuhn, D.J. Owen, B. Bader, A. Wittinghofer, J. Kuhlmann, H. Waldmann, J. Am. Chem. Soc. 123 (2001) 1023.
[68] E. Nagele, M. Schelhaas, N. Kuder, H. Waldmann, J. Am. Chem. Soc. 120 (1998) 6889.
[69] B. Bader, K. Kuhn, D.J. Owen, H. Waldmann, A. Wittinghofer, J. Kuhlmann, Nature (London) 403 (2000) 223.
[70] J. Tucker, G. Sczakiel, J. Feuerstein, J. John, R.S. Goody, A. Wittinghofer, EMBO J. 5 (1986) 1351.
[71] C. Lenzen, R.H. Cool, H. Prinz, J. Kuhlmann, A. Wittinghofer, Biochemistry 37 (1998) 7420.
[72] J. Jaumot, R. Gargallo, A. de Juan, R. Tauler, Chemometr. Intell. Lab. Syst. 76 (2005) 101.
[73] C. Kolano, Ph.D. Thesis, Fakultät für Chemie, Ruhr-Universität Bochum, 2003.
[74] C. Kötting, K. Gerwert, in: Erica A. Golemis, Peter D. Adams (Eds.), Protein–protein interactions, second ed., Cold Spring Harbor Lab. Press, 2005, pp. 279–299.

Characterization of the monolayer system

Determination of surface concentrations

The surface concentration is the projection of all molecules in the measured volume on the surface of the IRE (internal reflection element) and was calculated as described by Tatulian [1]. Briefly the surface concentration Γ was calculated by applying the thin-film theory with extinction coefficient ε, the number of internal reflections (N_r), number of equal functional groups (N_g) and the refractive indices of the IRE (n_1), the sample (n_2), and the medium (n_3) (n_{xy} equals n_x/n_y) as listed in Tab. S1 with equation 1. For the calculation of the surface concentration, polarized spectra were used and the integrated absorbances (A_{pp} and A_{vp}) of analyzed bands were calculated with a linear baseline and the integration-boundaries as listed in Tab. S1.

$$\Gamma = \frac{A_{pp} n_{12} \cos(\theta)}{N_g N_r \varepsilon \left(E_x^{\,2} E_z^{\,2}\right)} = \frac{A_{vp} n_{12} \cos(\theta)}{N_g N_r \varepsilon \left(E_y^{\,2}\right)} \qquad (1)$$

For this calculation the relative electrical field strengths E_x, E_y, and E_z relative to the experimental coordinate system of the ATR-crystal surface (Fig. S1) have to be known and were calculated according to equations 2a-c with the parameters angle of incidence (θ) and the refractive indices of the IRE (n_1), the thin layer sample (n_2), and the medium (n_3) which are listed in Tab S1.

$$E_x = \frac{2\cos\theta\sqrt{\sin^2\theta - n_{31}^2}}{\sqrt{1-n_{31}^2}\sqrt{\left(1+n_{31}^2\right)\sin^2\theta - n_{31}^2}} \qquad (2a)$$

$$E_y = \frac{2\cos\theta}{\sqrt{1-n_{31}^2}} \qquad (2b)$$

$$E_z = \frac{2\cos\theta\sin\theta n_{32}^2}{\sqrt{1-n_{31}^2}\sqrt{\left(1+n_{31}^2\right)\sin^2\theta - n_{31}^2}} \qquad (2c)$$

After the surface concentration was calculated from the polarized spectra A_{pp} and A_{vp} both values were combined with accounting the electric field intensities to yield isotropic values (A_{iso}) according to equation 3.

$$A_{iso} = \frac{A_{pp} + R_{iso} A_{vp}}{1 + R_{iso}} \qquad (3)$$

The isotropic dichroitic ratio R_{iso} represents the scaling factor of E_{pp} and E_{vp} and was calculated with equation 4.

$$R_{iso} = \frac{E_x^2 + E_z^2}{E_y^2} \qquad (4)$$

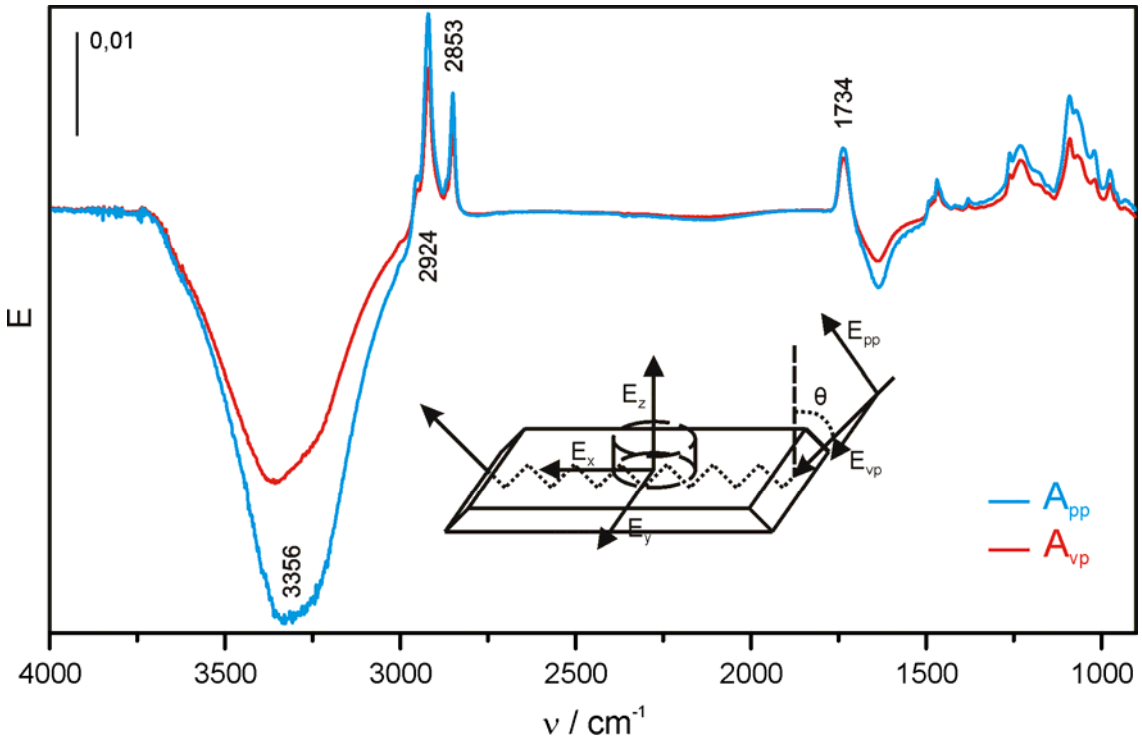

Fig. S1: Parallel and vertical polarized difference spectra (A_{pp}, A_{vp}) of the solid supported lipid bilayer preparation. The reference spectra were taken before incubation with lipid vesicles, thus bands facing upwards are caused by adsorbed lipid and bands facing downwards are caused by the displacement of water. The relative electric field strengths E_x, E_y, and E_z of the evanescent field can be derived from the electric field components E_{pp} and E_{vp} of the polarized IR beam, which in turn enables an orientational analysis of the bound lipids possible.

Lipid Surface concentration

The surface concentration of adsorbed lipids was calculated as described above from polarized difference spectra of the empty IRE and the IRE after the vesicle spreading process

was complete including a washing step to remove loosely bound vesicles (Fig. S1). The resulting value of 448 ± 57 pmol/cm^2 POPC is similar to values from literature of 460 pmol/cm^2 for a Langmuir-Blodgett film of POPC on top of a Germanium IRE [1] and 404 pmol/cm^2 for a doubled POPC monolayer (2 x 202 pmol/cm^2) generated with vesicle spreading on a LB-generated DPPA-monolayer [2]. Conversion into a mass-surface concentration yields 341 ± 43 ng/cm^2 which is also close to SPR results of SSLBs generated by vesicle spreading of 350 – 400 ng/cm^2 [3]. Further the area per lipid was calculated with the assumption that the lipids are organized in a bilayer. The resulting value of 75 ± 10 Å^2/lipid is close to the literature value from DOPC of 81 Å^2 [4].

Molecular orientation of the SSLB

As the ATR measurements during vesicle spreading are carried out in polarized mode it is possible to gain information on the molecular orientation of the emerging SSLB. The order parameters of the lipid alkane chains S_{lipid} and of the lipid carbonyl bond S_{CO} were calculated with equation 5, where E_x, E_y and E_z are the relative electric field strengths, and α is the angel between the transition dipole moment of the vibrational excitation and the molecular structure.

In case of S_{lipid} the transition dipole moment of the CH-groups is vertical to the axis of the lipid alkan chains, so that $\alpha = 90°$ was used for calculation; S_{CO} was calculated with $\alpha = 0°$.

$$S = \frac{2\left(E_x^2 - R_{\exp}E_y^2 + E_z^2\right)}{\left(3\cos^2\alpha - 1\right)\left(E_x^2 - R_{\exp}E_y^2 - 2E_z^2\right)} \qquad (5)$$

The experimental dichroitic ratio R_{exp} results from dividing the integrated absorbances of the CH-streching and the CO-streching bands of the lipid spectra in each polarisation respectively (A_{pp}/A_{vp}).

The order parameter used here is a value, which corresponds to an angle distribution with respect to the experimental z-axis (see Fig. S1). The order parameter which is –0.5 in case of 90°, 1 in case of 0°, and results in a value of 0 for isotropic orientation or an orientation of 54.7° (magic angle). Both, S_{CH} and S_{CO} are significantly different from 0, which indicates that the adsorbed lipids are part of an oriented structure. The S_{lipid} has a value of 0.2 ± 0.1 which is in between the literature values of NMR-derived order parameters of 0.15 – 0.2 for the Palmitoyl- and 0.1 for Oleyl-chain (Seelig and Seelig 1980). The lipid carbonyl function has an order paramter of –0.25 ± 0.04, which is similar to –0.18 - –0.26 found in multilayer films of DPPC and DMPC in the liquid disordered phase [5] and corresponds to an average angle β of the CO-bond relative to the IRE normal of 66 ± 9°.

The average angle β was calculated from the order parameter S by use of equation 6.

$$S = \frac{3\cos\beta - 1}{2} \qquad (6)$$

SSLB-thickness measured by AFM

Further we used atomic force microscopic (AFM) as an independent method to show that our method yields a single lipid bilayer. In these measurements a 10 µm x 10 µm area of the Germanium-IRE surface was measured in tapping mode with a WiTec alpha 300A (Ulm, Germany) atomic force microscope equipped with PNP-TR-tips (NanoAndMore, Wetzlar, Germany, 0.32 N/m, 67 kHz resonance frequency). The AFM experiments were done with the same buffer and IRE pre-treatment as used in the ATR-FTIR-experiments.

First the IRE was measured in buffer only. Afterwards the IRE was cleaned and a vesicle spreading experiment was performed with the ATR-FTIR setup as described above (see main text). After the SSLB was formed completely, the IRE was taken out of the cuvette. The whole procedure was done in buffer, so that no air could reach the SSLB. The Lipid-layer coated IRE was subsequently measured with the AFM again. The topography of both experiments is very similar. No adsorbed intact vesicles can be seen (Fig. S2 F and G). This shows first, that the vesicle spreading procedure results in a thin gapless layer, and second that the layer is so tightly associated with the IRE surface, that even the scratches from the polishing procedure are visible.

In a second experiment only a small amount of vesicles solution (1:50 of what is used in an ATR experiment) was incubated with the IRE for 10 min. After this the vesicle solution was exchanged by buffer and the surface was measured. In the resulting topography images (Fig S2 A) many small areas of 0.2 – 0.5 µm diameter can be seen which cover - together with a few larger regions of the same height – approximately 18% of the IRE surface. These regions were approximately 4 nm higher as the IRE surface (Fig S2 E), which is the same height as a POPC-bilayer [6]. Also filtering the image with respect to the z-values with cutoffs of < 2 nm, > 2 nm and > 6 nm shows, that the patches have the height of one but not more than one bilayer (Fig S2 B, C, D).

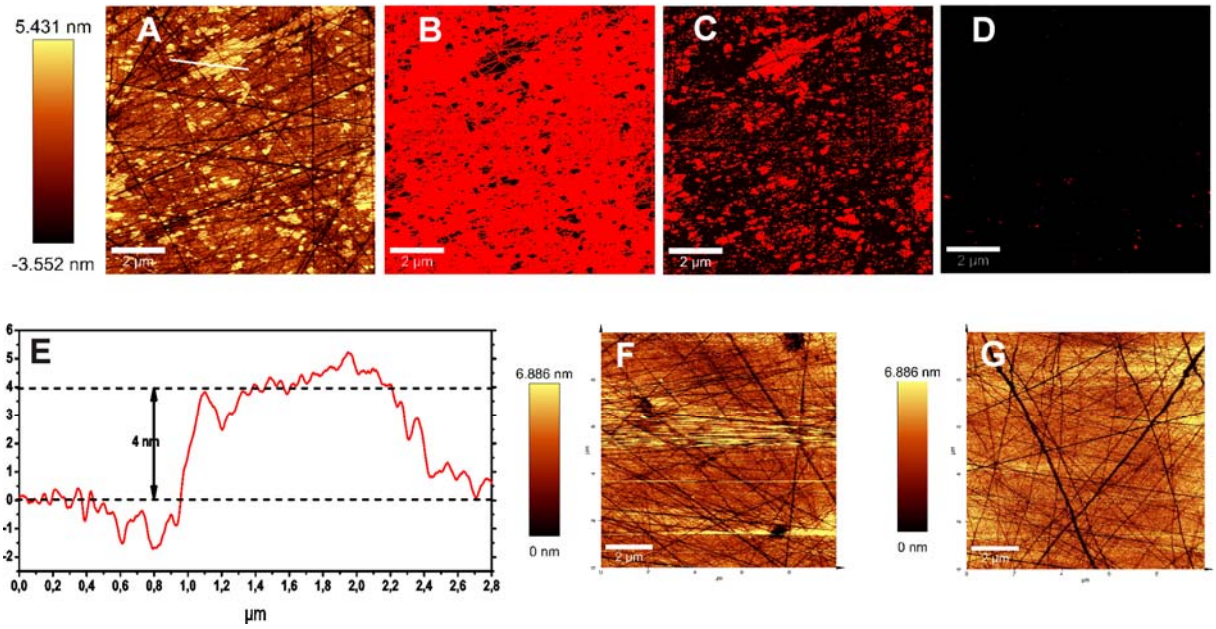

Fig. S2: AFM-investigation of the vesicle spreading on germanium-crystal surface
A: topography of substrate with cross section through spreaded lipidvesicles. B-D: selection of areas with z < 2 nm (B), z > 2 nm (C) and z > 6 nm (D) are shown in red. E: cross section through spreaded lipidvesicles shown in figure A, average width of cross section was 0.3 µm. F: topography of a germanium-crystal in buffer G: topography of a germanium-crystal with lipid membrane prepared in the ATR-FTIR spectrometer.

BSA adsorption as a SSLB-completeness-test

In monolayer adsorption studies it is of great importance to assure the native immobilisation of the sample protein. As adsorption of Ras directly to the underlying germanium support leads to denaturation of the protein it was checked if the POPC-SSLB is complete. For this, BSA (bovine serum albumine) was used as a marker molecule which strongly adsorbs at the Germanium surface, but not at a POPC-SSLB. First the reference spectrum was taken and then the surface was incubated with 0.8 µM BSA. The adsorption process was followed by measuring multiple spectra and plotting the absorbance of the amide II band (1548 cm^{-1}) against time (Fig S3). Assuming the maximum absorbance of BSA on Germanium of $9 \cdot 10^{-3}$ corresponds to a closed BSA-monolayer - because no further increase can be observed – the absorbance of $2 \cdot 10^{-4}$ of BSA on the SSLB-surface may be understood as BSA adsorption to remaining gaps in the SSLB. From this it can be concluded, that the formed SSLB is more than 98 % complete.

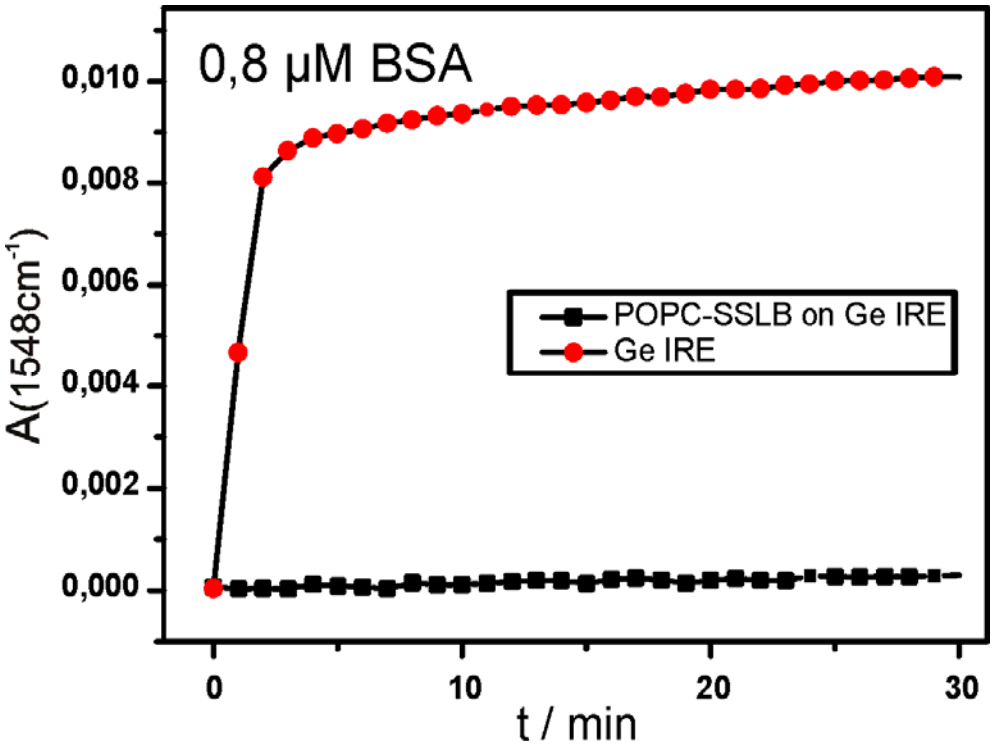

Fig S3: Adsorption of BSA on a hydrophilic germanium crystal (red) and on a POPC-SSLB (black) followed by the Amide II absorbance kinetics. BSA adsorbs at the germanium IRE but not at the POPC-SSLB, indicating that the layer is complete.

Adsorption of a protein monolayer of lipidated Ras

The adsorption of the lipidated Ras to the solid supported lipid bilayer was monitored with polarized ATR-FTIR. The resulting absorbance spectra of the bound Ras protein was used to calculated the surface concentration. For this purpose the amide II band was integrated and the surface concentration was calculated as described above. In a typical experiment the incubation of the SSLB surface with 5 µM Ras leads to a slow adsorption curve which gets constant after approximately 12 h and yields a final surface concentration of 13 ± 2 pmol/cm^2. This can be compared with a maximal theoretical Ras surface concentration of 16.6 pmol/cm^2, which can be deduced from the 3D-structure of the protein assuming a molecular area of 10 nm^2. Therefore the experimental value equates to a surface coverage of 78 %. Finally, the existence of partial Ras multilayers was excluded by adding an additional amount of Ras to an already complete saturated surface, which didn't cause an additional signal increase.

Table S1: Extinction coefficients, refractive indices, and other input parameters used for calculations

name	symbol	value	uncertainty	source
integrated molar absorption coefficients (cm/mol)				
ν(CH) (2990 – 2812 cm^{-1})	$\int \varepsilon_{CH} d\tilde{\nu}$	1.32×10^8	3.96×10^6	[1] uncertainty set to ~ 3 %
Amide II (1600 – 1485 cm^{-1})	$\int \varepsilon_{amideII} d\tilde{\nu}$	9.5×10^6	2.9×10^5	Obtained by own transmission measurements of Ras
refractive indices				
Germanium IRE	n_1	4	0.005	[1]
Lipid	n_2	1.43	0.04	[1] uncertainty set to ~ 3 %
protein	n_2	1.45	0.05	[7; 8]
H_2O	n_3	1.33	0.05	[1]
Other input parameters				
Angle of incidence (°)	θ	45	1.5	
active reflections	N_r	12.5	0.5	
Equal functional groups	N_g	189	0	number of residues of lipidated Ras

[1] S.A. Tatulian, Biochemistry 42 (2003) 11898-11907.
[2] G. Reiter, M. Siam, D. Falkenhagen, W. Gollneritsch, D. Baurecht, and U.P. Fringeli, Langmuir 18 (2002) 5761-5771.
[3] E. Reimhult, M. Zach, F. Hook, and B. Kasemo, Langmuir 22 (2006) 3313-3319.
[4] R.P. Rand, Annual Review of Biophysics and Bioengineering 10 (1981) 277-314.
[5] W. Hubner, and H.H. Mantsch, Biophysical Journal 59 (1991) 1261-1272.
[6] R. Richter, A. Mukhopadhyay, and A. Brisson, Biophysical Journal 85 (2003) 3035-3047.
[7] N. Hassler, D. Baurecht, G. Reiter, and U.P. Fringeli, Journal of Physical Chemistry C 115 (2011) 1064-1072.
[8] G. Reiter, N. Hassler, V. Weber, D. Falkenhagen, and U.P. Fringeli, Biochimica Et Biophysica Acta-Proteins and Proteomics 1699 (2004) 253-261.